

PCCP

Accepted Manuscript



This is an *Accepted Manuscript*, which has been through the Royal Society of Chemistry peer review process and has been accepted for publication.

Accepted Manuscripts are published online shortly after acceptance, before technical editing, formatting and proof reading. Using this free service, authors can make their results available to the community, in citable form, before we publish the edited article. We will replace this *Accepted Manuscript* with the edited and formatted *Advance Article* as soon as it is available.

You can find more information about *Accepted Manuscripts* in the [Information for Authors](#).

Please note that technical editing may introduce minor changes to the text and/or graphics, which may alter content. The journal's standard [Terms & Conditions](#) and the [Ethical guidelines](#) still apply. In no event shall the Royal Society of Chemistry be held responsible for any errors or omissions in this *Accepted Manuscript* or any consequences arising from the use of any information it contains.

**Anion and Cation Dynamics of Sulfonylamide-Based Ionic Liquids
and the Solid-Liquid Transitions.**

Mamoru Imanari,^a Kozo Fujii,^b Tomohiro Mukai,^c Noriko Mizushima,^d Hiroko Seki,^a
Keiko Nishikawa*,^b

^a Center for Analytical Instrumentation, Chiba University, Yayoi-cho, Inage-ku, Chiba 263-8522, Japan

^b Graduate School of Advanced Integration Science, Chiba University, Yayoi-cho, Inage-ku, Chiba 263-8522, Japan

^c Science Research Center, Hosei University, Fujimi, Chiyoda-ku, Tokyo 102-8160, Japan

^d Laboratory of Clinical Pharmacy, Yokohama College of Pharmacy, Matano-cho, Totsuka-ku, Yokohama 245-0066, Japan

Abstract

One of the important factors that characterise room-temperature ionic liquids (RTILs) is the variety of conformations adopted by the constituent ions and their flexibility. Using 1,3-dimethylimidazolium bis(fluorosulfonyl)amide ($[C_1mim][FSA]$) and 1,3-dimethylimidazolium bis(trifluoromethylsulfonyl)amide ($[C_1mim][NTf_2]$) as samples, the longitudinal and transverse relaxation times (T_1 and T_2) for ^{19}F and 1H were determined as a function of temperature and correlated to the dynamics of the phase behaviours of the two RTILs. Because the anions and cations in the two compounds have ^{19}F and 1H nuclei, respectively, the dynamics of each can be independently investigated and the relationships between them discussed. For $[C_1mim][FSA]$, the only observed phase changes included melting and crystallisation. The temperature dependence of T_1 and T_2 for ^{19}F was similar to that of T_1 and T_2 for 1H , indicating similar dynamics through the formation of strong anion–cation interactions. For $[C_1mim][NTf_2]$, the T_1 and T_2 values for both ^{19}F and 1H

discontinuously changed at same temperatures, which were assigned to the crystallisation and melting points. However, the T_1 curves for ^{19}F and ^1H were different in the crystalline region, suggesting independent dynamics for the anion and cation in $[\text{C}_1\text{mim}][\text{NTf}_2]$. In the crystalline state for each salt, the cation dynamics were distinctly separated into the framework movement of the imidazolium ring and the movement of the methyl groups, while the anion dynamics were characterised by the movement of the entire anion. The influence of the crystal structure on the dynamics of each salt was also considered.

1. Introduction

Room-temperature ionic liquids (RTILs) constitute a new class of liquids that has attracted much attention due to the characteristic properties¹⁻⁵ and potential utility of these materials as functional liquids.⁵⁻¹⁵ Unique properties are remarkably manifested in the thermal behaviours of RTILs, such as low melting points despite being composed only of ions, hardness upon crystallisation, pre-melting over a wide temperature range, excessive supercooling and complex thermal histories.¹⁶⁻²⁷ Extremely slow dynamics during phase changes is another characteristic phenomenon in many ionic liquids.^{23-25, 28, 29} These phenomena are proved to be closely related to the variety and flexibility of the conformations of the constituent ions.^{1, 30, 31} Many research groups have focused on cations of imidazolium-based RTILs and investigated phase behaviours linked to conformational changes of the substituent groups of each cation, using calorimetry,²²⁻²⁷ Raman spectroscopy^{1, 26, 27, 32-35} and nuclear magnetic resonance (NMR) analyses.^{29, 36-48} Previously, we revealed a relationship between the thermodynamic properties of imidazolium-based RTILs and their cation dynamics.^{22-27, 29, 44-48} However, studies on the flexibility of RTIL ions have mainly been limited to cations.

In the present study, attention was thus focused on the anion dynamics of sulfonamide-based RTILs to reveal the phase behaviours linked to those dynamics. The longitudinal and transverse relaxation times (T_1 and T_2 , respectively) for ^{19}F as a function of temperature were determined over a wide temperature range for RTILs with the two amide anions, bis(fluorosulfonyl)amide ($[\text{FSA}]^-$) and bis(trifluoromethylsulfonyl)amide ($[\text{NTf}_2]^-$) (see Figure 1 for the chemical structures). $[\text{FSA}]^-$ and $[\text{NTf}_2]^-$ are the most popular anions for RTILs. The cation 1,3-dimethylimidazolium ($[\text{C}_1\text{mim}]^+$) was used in both RTILs because it has no conformational flexibility other than the rotation of methyl groups around the N-C axes. Consequently, the flexibilities of the anion groups and the dynamics triggered by their flexible motions could be more easily investigated. In addition, the T_1 and T_2 values for ^1H were

measured. Specifically, because the anions and cations in the two RTILs have ^{19}F and ^1H nuclei, respectively, the dynamics of the anions and cations could be independently revealed and then the relationships between them evaluated.

Furthermore, these sulfonylamide anions are suggested to be highly non-coordinatable ions due to their broadly delocalised negative charges and large internal flexibility.^{49–52} Accordingly, by determining the ^1H and ^{19}F relaxation times, identifying the phase behaviours linked to differences in the anions should be possible.

2. Experimental

The samples, $[\text{C}_1\text{mim}][\text{FSA}]$ and $[\text{C}_1\text{mim}][\text{NTf}_2]$, were synthesised following a previously established procedure⁵³ as described in the Supporting Information of our recent paper.⁵⁴ The purity of the each sample was confirmed by ^1H and ^{13}C NMR and elemental analyses. No impurity signals were observed in the NMR spectra.

To determine the general thermal phase behaviours of the samples, calorimetric measurements of sufficiently dried samples (1–2 mg) were performed using a laboratory-made calorimeter with a baseline stability of $\pm 5 \mu\text{W}$ and a thermal stability of 0.001 K.³⁴ Measurements for both samples were performed at a scanning rate of 5 mK/s for the cooling and heating processes.

Samples for the NMR analyses were prepared by placing each neat RTIL (approximately 0.5–1 g) into a 10-mm-diameter glass sample tube. The sample was dried for 5 h at temperatures above 373 K under a 10^{-3} Pa vacuum to remove water and volatile contaminants that could affect the properties of the RTIL. After drying, each sample tube was flame-sealed under the connecting vacuum line.

The T_1 and T_2 measurements for ^{19}F and ^1H were performed using a JEOL MU-25 pulse NMR spectrometer with a ^{19}F resonance frequency of 23.5 MHz and a ^1H resonance

frequency of 25 MHz. At these low resonance frequencies, the overall dynamics of the anions and cations were observed because the separations of the signals according to the chemical shifts for each ion were small. The T_1 measurements were performed using the inversion recovery pulse sequence⁵⁵ and the saturation recovery method⁵⁶ for the states with long T_1 values. The T_2 measurements were performed using the Carr–Purcell–Meiboom–Gill (CPMG) pulse sequence for the liquid state^{57, 58} and the solid echo sequence for the solid state.^{59, 60} The temperature ranges for both samples were very wide. Each sample was first heated to a temperature 30–40 K higher than its melting point, then cooled down to a temperature 100–120 K lower than the melting point and subsequently warmed to the starting temperature. Measurements were performed every 10 K during which the sample was maintained at that temperature.

3. Results and discussion

3.1. Theoretical background

The homonuclear relaxation rates ($1/T_1$, $1/T_2$) are described using the following equations for the dipolar relaxation mechanism:^{61, 62}

$$\frac{1}{T_1} = \frac{2\gamma^4 \hbar^2 I(I+1)}{5r^6} \left[\frac{\tau_c}{1 + \omega^2 \tau_c^2} + \frac{4\tau_c}{1 + 4\omega^2 \tau_c^2} \right] \quad (1)$$

and

$$\frac{1}{T_2} = \frac{\gamma^2 \hbar^2 I(I+1)}{5r^6} \left[3\tau_c + \frac{5\tau_c}{1 + \omega^2 \tau_c^2} + \frac{2\tau_c}{1 + 4\omega^2 \tau_c^2} \right], \quad (2)$$

where ω is the ^{19}F or ^1H Larmor frequency, γ is the gyromagnetic ratio, \hbar is $h/2\pi$ with h representing Planck's constant, I is the spin quantum number, r is the inter-fluorine (or

-proton) distance and τ_c is the correlation time. The equations (1) and (2) can be applied for both ^{19}F and ^1H . The relaxation rate $1/T_1$ is proportional to τ_c in the region where $\omega\tau_c \ll 1$ (extreme narrowing condition) and is proportional to $1/\tau_c$ in the region where $\omega\tau_c \gg 1$. Consequently, the curve for T_1 vs. temperature in a phase has a positive slope in the higher temperature region and a negative slope in the lower temperature region, with the minimum value at $\omega\tau_c = 0.62$. On the other hand, because the relaxation rate $1/T_2$ is mainly proportional to τ_c in equation (2), the T_2 values simply decrease with a decrease in the temperature. If a phase change occurs, the T_1 and T_2 values should change discontinuously at that temperature. Furthermore, the temperature-dependent correlation time τ_c obeys the Arrhenius equation,⁵⁵

$$\tau_c = \tau_A \exp\left[\frac{E_a}{RT}\right], \quad (3)$$

where E_a is the activation energy, R is the gas constant and T is the absolute temperature. Therefore, the activation energy of reorientational motion can be estimated from the temperature dependence of the correlation time τ_c .

3.2. [C₁mim][FSA]

Calorimetric measurements for [C₁mim][FSA] were performed using a laboratory-made apparatus.³⁴ Crystalline [C₁mim][FSA] was first melted completely by heating, then cooled from 370 to 210 K and subsequently heated to 370 K. The cooling and heating rates were both 5 mK/s. The results are presented in Figure 2. The exothermic signal that appeared at approximately 303 K during cooling was assigned to the crystallisation process, while the endothermic signal observed at approximately 332 K during heating was attributed to the melting process. Notably for this sample, crystallisation occurred sharply during cooling and melting occurred over a relatively narrower temperature range than that typically seen for imidazolium-based ionic liquids with longer alkyl chains.^{22–27} In addition, no complex thermal histories were detected at the scanning rate used.

The NMR analyses for determining the ^{19}F T_1 and T_2 values for $[\text{C}_1\text{mim}][\text{FSA}]$ were performed over the temperature range from 233 to 413 K, varying the temperature by cooling from 413 to 233 K and then heating back to 413 K. At every 10 K, the measurements were performed keeping the temperature constant for each analysis. Figure 3 shows the obtained ^{19}F T_1 and T_2 values as a function of temperature. Both the ^{19}F T_1 and T_2 cooling curves (black curves) discontinuously changed at 303 K, which is the temperature assigned to the crystallisation process according to the calorimetric measurements (see Figure 2). After crystallisation, the T_1 values decreased as the temperature decreased, reaching a minimum at approximately 283 K. The correlation time for ^{19}F reorientational dynamics at 283 K was calculated to be approximately 4.2 ns using the relationship $\omega\tau_c = 0.62$ at the minimum point. After passing through the minimum point, the T_1 values then increased exponentially as the temperature decreased. On the other hand, the T_2 values remained nearly constant at 40 μs after the crystallisation. During heating (red symbols), the ^{19}F T_1 and T_2 values followed the corresponding T_1 and T_2 traces for the cooling process except in the super-cooled region from 303 to 333 K and discontinuously changed at approximately 333 K. This temperature corresponds to the melting temperature observed in the calorimetric measurements (see Figure 2). After melting, both the ^{19}F T_1 and T_2 values perfectly followed the corresponding T_1 and T_2 traces obtained during cooling.

The ^1H T_1 and T_2 values for $[\text{C}_1\text{mim}][\text{FSA}]$ as a function of temperature are shown in Figure 4. Like the temperature dependence curves of the ^{19}F T_1 and T_2 values, the ^1H T_1 and T_2 curves changed discontinuously at approximately 303 K during cooling and 333 K during heating, the temperatures assigned to the crystallisation and melting processes, respectively. In addition, in the crystalline state, the value of ^1H T_1 reached a minimum at the same temperature as that for ^{19}F T_1 , and the ^1H T_2 values remained constant at 22 μs . The temperature dependence curves of the ^1H T_1 and T_2 values during heating (red symbols) also

behaved similarly to those obtained during cooling (black symbols), except in the super-cooled region. The activation energy estimated from the linear part of the ^1H T_1 trace during heating was 12.9 kJ/mol. This value corresponds well to the rotational energy of the C–CH₃ axis in [C₄mim]Cl determined using inelastic neutron scattering experiments.⁶³ Therefore, it is possible to conclude that the correlation time $\tau_c = 3.95$ ns derived from the T_1 minimum point at approximately 283 K is associated with the rotational motion of methyl groups in the crystalline phase.

Comparing the cooling curves for ^{19}F T_1 (black closed squares in Figure 3) and ^1H T_1 (black closed squares in Figure 4), it can be seen that the values for ^1H in the liquid state jumped to higher values during the phase change to the crystalline state at 303 K, while those for ^{19}F jumped to lower values. Moreover, the discontinuity for ^1H T_1 at the phase change was more remarkable than that for ^{19}F T_1 . These results are interpreted as follows. If neglecting the interactions between ions is possible, then the observed correlation time (τ_{obs}) can be separated into two contributions,

$$1/\tau_{\text{obs}} = 1/\tau_{\text{frame}} + 1/\tau_{\text{local}}, \quad (4)$$

where τ_{frame} and τ_{local} are the correlation times from the frame of the ion and the internal local motion in the ion, respectively. In the [C₁mim] cation, τ_{frame} corresponds to the correlation time for the imidazolium ring, and this value became very large at the crystallisation point. Therefore, the longitudinal relaxation time $T_{1,\text{frame}}$ due to the dipole–dipole interaction, which is given by equation (1), became very large. Consequently, in the observed values ($T_{1,\text{obs}}$) given by following relationship:

$$1/T_{1,\text{obs}} = 1/T_{1,\text{frame}} + 1/T_{1,\text{local}}, \quad (5)$$

$1/T_{1,\text{frame}}$ can be neglected. The parameter $T_{1,\text{local}}$ corresponds to the contribution from the rotation of the methyl groups. Figure 4 shows that only the contribution from the methyl groups appears in the T_1 curve in the crystalline state and the methyl groups in the cation

move actively even after crystallisation, while the frame of the cation, namely the imidazolium ring, is frozen. The activation energy of the rotation of the methyl groups was 12.9 kJ/mol, as described above. For the [FSA] anion, on the other hand, distinctly separating the frame and local parts according to their movements was impossible.

Aside from the above-mentioned trend, the behaviours of the temperature-dependent ^1H T_1 and T_2 curves, namely the crystallisation and melting points and minimum T_1 values, were in perfect agreement with those observed for the ^{19}F T_1 and T_2 curves. The correlation time for ^{19}F at 283 K was approximately 4.2 ns, which is very close to the ^1H correlation time of 3.95 ns. These results suggested the same dynamics of the anion and the cation due to the formation of strong interactions.

Recently we reported the crystal structure of $[\text{C}_1\text{mim}][\text{FSA}]$ determined via single-crystal X-ray diffraction.⁵⁴ Therefore, the dynamics of the salt in the crystalline state were considered in relation to the crystal structure. First, the magnitudes of the ^{19}F T_1 values were compared before and after crystallisation. The ^{19}F T_1 values were nearly the same for the liquid and crystalline states, although ^{19}F T_2 showed clearly a discontinuous change. In the crystalline state, the conformation of the $[\text{FSA}]^-$ ion is a perfectly symmetric cisoid,⁵⁴ while transoid conformers are partially included in the liquid state as described later. As a result, the averaged internal distance between F atoms for the liquid state is longer than the one for the crystalline state. Because the value of T_1 is proportional to the sixth power of the distance between dipoles as shown in equation (1), the ^{19}F T_1 values for the liquid state are larger. This is the reason why the jump of ^{19}F T_1 values at the crystallisation became smaller.

Second, the contribution of hydrogen bonding was evaluated. As noticed in Figures 5(a) and (b), the structure of the crystal is characterised by three types of hydrogen bonds.⁵⁴ The strongest hydrogen bond in the crystal is formed between two O atoms in an anion and three H atoms in a cation to generate a characteristic W-shaped tridentate bonding arrangement (see

Figure 5(a)). The second strongest hydrogen bond is formed between two O atoms in an anion and two of the H atoms attached to an imidazolium ring of a cation. As seen in Figure 5 (b), two O atoms in an anion also form weaker hydrogen bonds with two H atoms in the methyl groups of a cation to form the third and weakest type of hydrogen bond. Surprisingly, no F atoms take part in the hydrogen bonding. N(SO₂R)₂-type anions are well known to be characterised by the large flexibility of the SO₂ groups around the S–N axes.^{52, 64, 65} However, for [C₁mim][FSA], the movement of the SO₂ groups in the anion is hindered by the strong hydrogen bonds with the cation. The motion of the F atoms is also restricted, because each F atom is directly bonded to each S atom. The motion of the methyl groups in the cation is also hindered. Furthermore, all three types of hydrogen bonding can occur between a single anion and a single cation, as shown in Figures 5 (a) and (b). In such a way, the anion and cation are connected with very rigid and strong interactions, which were reflected in the similar reorientational dynamics observed for the cation and anion of [C₁mim][FSA] in the crystalline state. Even in the liquid state, imagining that the anion and cation form strong pairs is possible due to the strong hydrogen bonding that occurs between them in addition to Coulomb interactions.

Looking again at Figures 3 and 4, it can be seen that after passing through the minimum point, both the ¹⁹F and ¹H *T*₁ values increased exponentially as the temperature decreased to large values of 15 and 20 s, respectively, at 223 K. These values are extremely large compared to those for crystalline [C₁mim][NTf₂] as described later and [C_{*n*}mim]Br^{29, 43, 44} and suggest that [C₁mim][FSA] forms a hard crystal due to the ordering of the constituent ions with high symmetries and the strong hydrogen bonding⁵⁴ described above.

Using Raman spectroscopy, two stable conformers of the [FSA][−] ion, cisoid and transoid, were confirmed to coexist in the liquid state of [C₁mim][FSA], as is the case with [C₂mim][FSA].⁵² On the other hand, in the crystalline state, [C₁mim][FSA] only adopts the

cisoid conformation.⁵⁴ Therefore, the phase transition (melting during heating) and structural relaxation (crystallisation during cooling) of [C₁mim][FSA] can be concluded to occur due to the cisoid/transoid conformational change of a portion of [FSA]⁻ ions.

3.3. [C₁mim][NTf₂]

The calorimetric data for [C₁mim][NTf₂] are presented in Figure 6. The exothermic signal at 283 K during cooling and the endothermic signal at 298 K during heating were assigned to the crystallisation and melting points, respectively. Like for [C₁mim][FSA], crystallisation of [C₁mim][NTf₂] occurred sharply during cooling, and no complex thermal histories were detected with a scanning speed of 5 mK/s. Although a pre-melting phenomenon was observed, the temperature range was relatively narrow compared with those of imidazolium-based ionic liquids with longer alkyl chains, such as [C₄mim]⁺ salts²²⁻²⁷. In addition, the temperature range of the supercooled region was 15 K under the experimental conditions used in the present study and was relatively narrower than those of imidazolium-based RTILs with the cation flexibility.

The ¹⁹F *T*₁ and *T*₂ values plotted as a function of temperature in Figure 7 revealed the dynamics of the anion in [C₁mim][NTf₂]. They both discontinuously changed at approximately 283 K during cooling (black symbols in Figure 7) and 303 K during heating (red symbols in Figure 7), which correspond to the crystallisation and melting temperatures, respectively. Note that the change in the ¹⁹F *T*₁ values after crystallisation was only slight in the range from 280 to 240 K. Hence, clearly identifying a minimum value for *T*₁ was not possible. This behaviour suggests the presence of plural *T*₁ minima distributed over a wide temperature range due to the flexibility around the two N–S and S–CF₃ axes of the [NTf₂]⁻ ion in the crystalline state. All of the [NTf₂]⁻ ions in [C₁mim][NTf₂] have been reported to adopt the cisoid conformation in the crystalline state.⁶⁶ The flexibility of the [NTf₂]⁻ ion has been suggested by the small energy differences associated with large geometrical variations.⁶⁷

⁶⁸ Therefore, it is possible that even in the crystalline state of [C₁mim][NTf₂], the cisoid conformation is an average conformation, and the [NTf₂]⁻ ions move with large amplitudes.

The ¹H T_1 and T_2 values for [C₁mim][NTf₂] as a function of temperature are plotted in Figure 8. Discontinuous changes in these values occurred near 283 and 303 K, which are the same temperatures observed for the ¹⁹F T_1 and T_2 curves and correspond to the crystallisation and melting processes, respectively. After crystallisation, the T_1 values linearly (on a logarithmic scale in Figure 8) decreased to a minimum at 213 K as the temperature decreased. Unlike for the ¹⁹F T_1 curve, however, only one minimum point was recognised, which suggested that the two methyl-groups in the cation likely had the same dynamics. In addition, the temperature of the ¹H T_1 minimum point for [C₁mim][NTf₂] was lower than that for [C₁mim][FSA], and the activation energy for [C₁mim][NTf₂] (estimated from the linear part of the T_1 curve from 233 to 293 K) of approximately 8.7 kJ/mol was also less than that for [C₁mim][FSA]. This smaller value indicated that in the crystalline state, the methyl groups in the cation of [C₁mim][NTf₂] could move more easily than those in the cation of [C₁mim][FSA].

Similar to the behaviour observed for [C₁mim][FSA], the ¹H T_1 values for [C₁mim][NTf₂] during cooling (black closed squares in Figure 8) jumped to higher values during the phase change from the liquid to the crystalline state at 283 K, while the ¹⁹F T_1 values (black closed squares in Figure 7) jumped to lower values. The explanation for these trends is also similar to that given for [C₁mim][FSA]. The imidazolium moiety and the methyl groups are distinctly separate from the viewpoint of movement. The imidazolium ring position is frozen at the time of crystallisation, while the methyl groups can still rotate. Therefore, the rotation of the methyl groups in the crystalline state is the only contribution that the cation in [C₁mim][NTf₂] makes to the ¹H T_1 (see Eq. (5)). In contrast, in the [NTf₂]⁻ ion, the entire ion moves, because the CF₃SO₂ groups rotate around the N–S axes and the CF₃ groups rotate around the S–C

axes. Therefore, separating the movement of the anion into the individualised movements of the different groups is impossible.

Furthermore, note that the jump width for the ^{19}F T_1 values of $[\text{C}_1\text{mim}][\text{NTf}_2]$ (Figure 7) was remarkably wider than that for the ^{19}F T_1 values of $[\text{C}_1\text{mim}][\text{FSA}]$ (Figure 3). This result indicated that the motions of the F atoms were likely different in the liquid and crystalline states due to an increase in bulkiness resulting from the exchange of F atoms for CF_3 groups.

Holbrey *et al.* reported the crystal structure of $[\text{C}_1\text{mim}][\text{NTf}_2]$.⁶⁶ Because structural information provides a more detailed understanding of the dynamics of the salt, the features of the structure were considered with respect to the results obtained in the present study. The arrangement of the $[\text{NTf}_2]^-$ ions around a $[\text{C}_1\text{mim}]^+$ ion, shown in Figure 9, is based on the crystal data by Holbrey *et al.*,⁶⁶ with a focus on the structural interactions between the cation and anion due to hydrogen bonding. In the crystalline state, the $[\text{NTf}_2]^-$ ion adopts a slightly distorted cisoid conformation. Similar to the structure of crystalline $[\text{C}_1\text{mim}][\text{FSA}]$, the structure of the $[\text{C}_1\text{mim}][\text{NTf}_2]$ crystal is characterised by three types of hydrogen bonds. The strongest hydrogen bond in the crystal is formed with two O atoms from the anion and three H atoms in the cation to generate a characteristic W-shaped tridentate hydrogen bonding arrangement, although it is slightly distorted (see Figure 9). The second strongest hydrogen bond is formed with two O atoms from different anions and two H atoms bonded directly to an imidazolium ring. Both of these types of hydrogen bonds are formed in the imidazolium plane. As shown in Figure 9, a third, weaker hydrogen bond is formed between two O atoms in different anions with two H atoms in the methyl groups in a single cation. In addition, as is the case for crystalline $[\text{C}_1\text{mim}][\text{FSA}]$, no F atoms participate in the hydrogen bonding in crystalline $[\text{C}_1\text{mim}][\text{NTf}_2]$. There are, however, two differences in the crystal structures of $[\text{C}_1\text{mim}][\text{FSA}]$ (Figure 5 (a) and (b)) and $[\text{C}_1\text{mim}][\text{NTf}_2]$ (Figure 9): (i) in the $[\text{C}_1\text{mim}][\text{NTf}_2]$ crystal, other than in the W-shaped hydrogen bond, the $[\text{C}_1\text{mim}]^+$ ion forms hydrogen bonds

with multiple anions, while in the $[\text{C}_1\text{mim}][\text{FSA}]$ crystal, the $[\text{C}_1\text{mim}]^+$ ion forms the 1:1 pair with the anion for each hydrogen bonding that is characterized by polydentate hydrogen bonding and ii) the F atoms in the $[\text{C}_1\text{mim}][\text{NTf}_2]$ crystal can move relatively easily via rotation of the CF_3 groups because there is no restriction due to hydrogen bonding, while movement of the F atoms in $[\text{C}_1\text{mim}][\text{FSA}]$ is restricted due to the strong hydrogen bonding of the SO_2 groups, which are directly bonded to the F atoms. According to the packing structure, the CF_3 groups gather and form a sheet structure in the $[\text{C}_1\text{mim}][\text{NTf}_2]$ crystal,⁶⁶ and thus each CF_3 group exists in the weaker interaction field formed by other CF_3 groups. Hence, the F atoms in $[\text{C}_1\text{mim}][\text{NTf}_2]$ are thought to be able to move more freely.

Finally, both the ^{19}F T_1 and ^1H T_1 values for $[\text{C}_1\text{mim}][\text{NTf}_2]$ and $[\text{C}_1\text{mim}][\text{FSA}]$ gradually increased as the temperature decreased below 210 K due to a decrease in flexibility. However, the values for the $[\text{C}_1\text{mim}][\text{NTf}_2]$ crystal were much smaller than those for the $[\text{C}_1\text{mim}][\text{FSA}]$ crystal, which suggests that the former is much softer than the latter at the same temperature. This difference is thought to be due to the differences in the hydrogen bonding in the two RTILs as mentioned above in (i) and (ii).

Conclusions

Calorimetric data and the temperature dependence of the NMR relaxation times (T_1 and T_2) for the RTILs $[\text{C}_1\text{mim}][\text{FSA}]$ and $[\text{C}_1\text{mim}][\text{NTf}_2]$ were evaluated. The ^{19}F relaxation times were suitable probes for studying the anion ($[\text{FSA}]^-$ and $[\text{NTf}_2]^-$) dynamics of the samples, while the behaviour of the ^1H relaxation times independently revealed the dynamics of the cation ($[\text{C}_1\text{mim}]^+$) in each RTIL. This data was then used to discuss the relationships between these behaviours. For both the samples, although the thermal histories observed according to the calorimetric and NMR analyses were different, the phase change temperatures determined in the calorimetric experiments agreed well with the temperatures at which the T_1 and T_2

values exhibited discontinuities. The results also indicated that each samples had a minimal thermal history.

With regard to [C₁mim][FSA], crystallisation from the liquid state occurs due to a conformational change of the anions; namely, the portion of anions that exist in the transoid conformation in the liquid state change to the cisoid conformation. At the same time, the systematic arrangement of the imidazolium cations occurs, because they are bound tightly with the cisoid anions. The melting process involves the opposite transformations. In addition, the methyl groups in the cation move even in the crystalline state, at least down to 210 K, with an estimated activation energy of 12.9 kJ/mol. Furthermore, the T_1 values for ¹⁹F in the crystalline state are not very different from those for ¹⁹F in the liquid state, suggesting that, with respect to the librational motion around the cisoid arrangement in the crystalline state, the SO₂F groups move to the same extent as they do in the liquid state. Finally, on the whole, the cation and anion exhibit cooperative motion, likely due to strong hydrogen bonding interactions.

With regard to [C₁mim][NTf₂], crystallisation and melting are also caused by changes between the transoid and cisoid forms. However, there are two types of rotational freedom in the [NTf₂]⁻ ion, namely rotation around the N–S axes and CF₃ rotation. In the crystalline state, the overlap of these two types of rotational dynamics was observed in the T_1 behaviours. In addition, as with crystalline [C₁mim][FSA], the methyl groups in the cation of [C₁mim][NTf₂] were found to move in the crystalline state, even at 210 K. However, the activation energy for [C₁mim][NTf₂] was significantly lesser than that for [C₁mim][FSA] at 8.7 kJ/mol. Judging from both the ¹⁹F and ¹H T_1 values, the former crystal can be concluded to be much softer than the latter. These differences are likely due to differences in the hydrogen bonding interactions in the two RTILs and their free volumes, which are due to the different efficiencies of cation and anion packing. Specifically, for [C₁mim][FSA], the

volumes of the cation and the anion are nearly the same and thus very efficient and close packing is achieved in the crystalline state.⁵⁴

Furthermore, note that sulfonylamide anions have conformational variations and flexibilities. The resultant and characteristic softness results in unique and effective functionality for these ionic groups as constituent anions in ionic liquids. The present study is one of a series of fundamental studies designed to reveal the dynamics of ionic liquids, including those with the simplest [FSA]⁻ and second simplest [NTf₂]⁻ ions and their related phase behaviours.

Acknowledgments

This work was partially supported by MEXT KAKENHI (Grant Number: 17073002) and JSPS KAKENHI (Grant Number: 24655003). The NMR experiments for ¹H and ¹⁹F were performed in Center for Analytical Instrumentation of Chiba University and in JEOL Ltd., respectively. The authors express sincere thanks for Mr. Masahisa Sawada and Mr. Takeyoshi Ikeda of JEOL Ltd. for improvement of the MU-25 NMR apparatus for the present study.

References

- 1 H. Hamaguchi and R. Ozawa, *Adv. Chem. Phys.*, 2005, **131**, 85–104.
- 2 Physical Chemistry of Ionic Liquids, Special issue of *J. Phys. Chem. B*, ed. J. F. Wishart and E. W. Castner, Jr., 2007, **111**, No. 18.
- 3 Ionic Liquids, Special issue of *Acc. Chem. Res.*, ed. R. D. Rogers and G. A. Voth, 2007, **40**, No.11.
- 4 J. F. Wishart and E. W. Castner, Jr. *J. Chem. Phys.*, 2010, **132**, No. 120901.
- 5 *Science of Ionic Liquids*, ed. K. Nishikawa, Y. Ouchi, T. Itoh, H. Ohno and M. Watanabe, Maruzen, Tokyo, Japan, 2012 (in Japanese).
- 6 T. Welton, *Chem. Rev.*, 1999, **99**, 2071–2083.
- 7 M. J. Earle and K. R. Seddon, *Pure Appl. Chem.* 2000, **72**, 1391–1398.
- 8 J. S. Wilkes, *Green Chem.*, 2002, **4**, 73–80.
- 9 *Ionic Liquids – Industrial Applications for Green Chemistry*, ed. R. D. Rogers and K. R. Seddon, A.C.S. Symp. Ser. 818, Am. Chem. Soc., Washington DC, 2002.
- 10 *Ionic Liquids in Syntheses*, ed. P. Wasserscheid and T. Welton, VCH-Wiley, Weinheim, Germany, 2003.
- 11 J. Dupont, R. F. de Souza and P. A. Z. Suarez, *Chem. Rev.*, 2002, **102**, 3667–3692.
- 12 T. Welton, *Coord. Chem. Rev.*, 2004, **248**, 2459–2477.
- 13 *Electrochemical Aspects of Ionic Liquids*, ed. H. Ohno, Wiley-Interscience, Hoboken, 2005.
- 14 N. V. Plechkova and K. R. Seddon, *Chem. Soc. Rev.*, 2008, **37**, 123–150.
- 15 T. L. Greaves and C. J. Drummond, *Chem. Rev.*, 2008, **108**, 206–237.
- 16 J. D. Holbray and K. R. Seddon, *J. Chem. Soc. Dalton Trans.*, 1999, **13**, 2133–2139.
- 17 H. L. Ngo, K. LeCompte, L. Hargens, A. B. McEwen, *Thermochim. Acta*, 2000,

- 357, 97–102.
- 18 Huddleston, J. G.; Visser, A. E.; Reichert, W. M.; Willauer, H. D.; Broker, G. A.; Rogers, R. D. *Green Chem.* 2001, **3**, 156–164.
- 19 C. P. Fredlake, J. M. Crosthwaite, D. J. Hert, S. N. V. K. Aki and S. N. Brennecke, *J. Chem. Eng. Data* 2004, **49**, 954–964.
- 20 Y.U. Paulechka, G.J. Kabo, A.V. Blokhin, A.S. Shaplov, E.I. Lozinskaya and Ya.S. Vygodskii, *J. Chem. Thermodynamics*, 2007, **39**, 158-166.
- 21 Marsh, K. N.; Boxall, J. A.; Lichtenthaler, R. *Fluid Phase Equilibria*, 2004, **219**, 93–98.
- 22 K. Nishikawa, S. Wang, H. Katayanagi, S. Hayashi, H. Hamaguchi, Y. Koga and K. Tozaki, *J Phys. Chem B*, 2007, **111**, 4894–4900.
- 23 K. Nishikawa, S. Wang and K. Tozaki, *Chem. Phys. Lett.*, 2008, **458**, 88–91.
- 24 K. Nishikawa and K. Tozaki, *Chem. Phys. Lett.*, 2008, **463**, 369–372.
- 25 K. Nishikawa, S. Wang, T. Endo and K. Tozaki, *Bull. Chem. Soc. Jpn.*, 2009, **82**, 806–812.
- 26 Endo, T.; Kato, T.; Tozaki, K.; Nishikawa, K. *J. Phys. Chem. B*, 2010, **114**, 407–411.
- 27 T. Endo, T. Kato and K. Nishikawa, *J. Phys. Chem. B*, 2010, **114**, 9201–9208.
- 28 Shamin N.; McKenna, G. B. *J. Phys. Chem. B*, 2010, **114**, 15942–15952.
- 29 M. Imanari, K. Fujii, T. Endo, H. Seki, K. Tozaki and K. Nishikawa, *J. Phys. Chem. B*, 2012, **116**, 3991–3997.
- 30 J. D. Holbrey, W. M. Reichert, M. Nieuwenhuyzen, S. Johnston, K. R. Seddon, R. D. Rogers, *Chem. Commun.*, **2003**, 1636–1637.
- 31 S. Hayashi, R. Ozawa, H. Hamaguchi, *Chem. Lett.* **2003**, 32, 498–499.
- 32 Ozawa, R.; Hayashi, S.; Saha, S.; Kobayashi, A.; Hamaguchi, H. *Chem. Lett.* **2003**, 32, 948–949.

- 33 Berg, R. W. *Monatsh. Chem.*, 2007, **138**, 1045–1075, and references cited therein.
- 34 T. Endo, K. Tozaki, T. Masaki, and K. Nishikawa, *Jpn J. Appl. Phys.* 2008, **47**, 1775–1779
- 35 Endo, T.; Nishikawa, K. *J. Phys. Chem. A*, 2008, **112**, 7543–7550.
- 36 Y. Dong, *Prog. Nucl. Magn. Reson. Spectrosc.* 2002, **41**, 115–151.
- 37 D. Bankmann and R. Giernoth, *Prog. Nucl. Magn. Reson. Spectrosc.* 2007, **51**, 63–90.
- 38 J. H. Ansony, D. T. Mertens, A. Dölle. P. Wasserscheid and W. G. Carper, *ChemPhysChem*, 2003, **4**, 588–594.
- 39 J. H. Ansony, D. Mertens, T. Breitenstein, A. Dölle. P. Wasserscheid and W. R. Carper, *Pure Appl. Chem.* 2004, **76**, 255–261.
- 40 W. R. Carper, P. G. Wahlbech and A. Dölle. *J. Phys. Chem. A*, 2004, **108**, 6096–6099
- 41 S. H. Chung, R. Lopato, S. G. Greenbaum, H. Shirota, E. W. Castner Jr, and J. F. Wishart, *J. Phys. Chem. B* 2007, **111**, 4855–4893.
- 42 K. Hayamizu, S. Tuzuki and S. Seki, *J. Phys. Chem. A*, 2008, **112**, 12027–12036.
- 43 M. Imanari, M. Nakakoshi, H. Hiroko and K. Nishikawa, *Chem. Phys. Lett.* 2008, **459**, 89–93.
- 44 M. Imanari, K. Uchida, K. Miyano, H. Seki and K. Nishikawa, *Phys. Chem. Chem. Phys.* 2010, **12**, 2959–2967.
- 45 T. Endo, M. Imanari, H. Seki and Keiko Nishikawa, *J. Phys. Chem. A* 2011, **115**, 2999–3005.
- 46 T. Endo, S. Widgeon, P. Yu, S. Sen and K. Nishikawa, *Phys. Rev. B* 2012, **85**, 054307-1~ -9.
- 47 T. Endo, H. Murata, M. Imanari, N. Mizushima, H. Seki and K. Nishikawa, *J. Phys.*

- Chem. B* 2012, **116**, 3780–3788.
- 48 T. Endo, H. Murata, M. Imanari, N. Mizushima, H. Seki, S. Sen and K. Nishikawa
J. Phys. Chem. B 2013, **117**, 326–332.
- 49 J. Foropoulos, D. D. DesMarteau, *Inorg. Chem.* 1984, **23**, 3720–3723.
- 50 P. Johansson, J. Tegenfeldt and J. Lindgren, *J. Phys. Chem. A* 2000, **104**, 954–961.
- 51 J. D. Holbrey, W. M. Reichert and R. D. Rogers, *Dalton Trans.*, 2004, 2267–2271.
- 52 K. Fujii, A. Seki, S. Fukuda, R. Kanzaki, T. Takamuku, Y. Umebayashi, and
S. Ishiguro, *J. Phys. Chem., B* 2007, **111**, 12829–12833.
- 53 P. Bonhôte, A. P. Dias, N. Papageorgiou, K. Kalyanasundaram, M. Grätzel, *Inorg.
Chem.*, 1996, **35**, 1168–1178.
- 54 K. Fujii, T. Mukai, and K. Nishikawa, *Chem. Lett.* 2014, **43**, 405–407.
- 55 T. C. Farrar and E. D. Becker, *Pulse and Fourier Transform NMR, Introduction to
Theory and Method*, Academic Press, New York, 1971.
- 56 J. L. Markley, W. J. Horsley, M.P. Klein, *J. Chem. Phys.* 1971, **55**, 3604–3605.
- 57 H. Y. Carr, E. M. Purcell, *Phys. Rev.* 1954, **94**, 630–642,
- 58 S. Meiboom and D. Gill, *Rev. Sci. Instrum.*, 1958, **29**, 688–691.
- 59 P. Mansfield, *Phys. Rev.* 1965, **137**, 961–974
- 60 J. G. Powels and J. H. Streng, *Proc. Phys. Soc.* 1963, **82**, 6–15.
- 61 N. Bloembergen, E. M. Purcell, R. V. Pound, *Phys. Rev.* 1948, **73** 679–712.
- 62 I. Solomon, *Phys. Rev.* 1955, **99**, 559–565
- 63 Y. Inamura, O. Yamamuro, S. Hayashi and H. Hamaguchi, *Physica B: Condensed
Matter* 2006, **385–386**, 732–734.
- 64 L. Xue, C. W. Padgett, D. D. DesMarteau, W. T. Pennington, *Solid State Sci.* 2002, **4**,
1535–1545.
- 65 J. N. C. Lopes, K. Shimizu, A. A. H. Padua, Y. Umebayashi, S. Fukuda, K. Fujii,

- S. Ishiguro, *J. Phys. Chem. B* 2008, **112**, 9449–9445.
- 66 J. D. Holbrey, W. M. Reichert and R. D. Rogers, *Dalton Trans.*, 2004, 2267–2271
- 67 P. Johansson, S. P. Geijji, J. Tegenfeldt and J. Lindgren, *Electrochimica Acta*, 1998, **43**, 1375–1379.
- 68 M. Herstedt, M. Smirnov, P. Johansson, M. Chami, J. Grondin, L. Servant, J. C. Lassegues, *J. Raman Spectrosc.* 2005, **36**, 762–770.

Figure captions

Figure 1. Chemical structures of the cation ($[\text{C}_1\text{mim}]^+$) and anions ($[\text{FSA}]^-$ and $[\text{NTf}_2]^-$).

Figure 2. Calorimetric curve for $[\text{C}_1\text{mim}][\text{FSA}]$ obtained using a laboratory-made calorimeter. The scanning rate for cooling and heating was 5 mK/s. The crystalline sample was first melted completely by heating, then cooled from 370 to 210 K and finally heated to 370 K. The sharp exothermic signal, at approximately 303 K during the cooling process, was assigned to crystallisation; the endothermic signal, at approximately 332 K during the heating process, was attributed to melting.

Figure 3. ^{19}F T_1 and T_2 values for $[\text{C}_1\text{mim}][\text{FSA}]$ as a function of temperature obtained using a ^{19}F pulse NMR spectrometer. The temperature was varied according to the following cycle: cooling from 413 to 233 K followed by heating to 413 K. Measurements were obtained every 10 K, keeping the temperature constant. The discontinuous points in the T_2 curve near 303 K during cooling and 333 K during heating correspond to the crystallisation and melting points, respectively.

Figure 4. ^1H T_1 and T_2 values for $[\text{C}_1\text{mim}][\text{FSA}]$ as a function of temperature obtained using a ^1H pulse NMR spectrometer. The temperature was varied in the same manner as described in Figure 3.

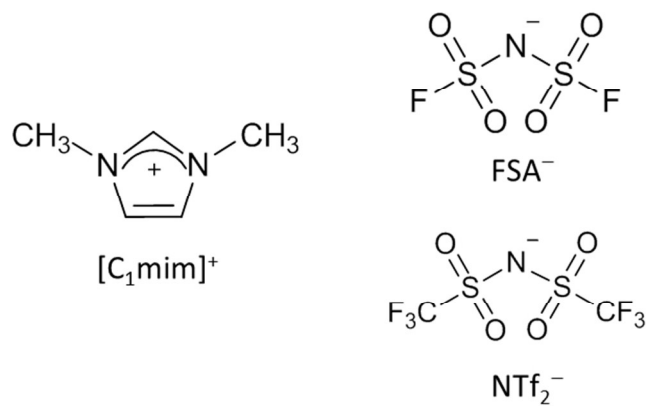
Figure 5. (a) In-plane hydrogen bonding and (b) out-of-plane hydrogen bonding in a $[\text{C}_1\text{mim}][\text{FSA}]$ crystal. Grey: carbon, blue: nitrogen, yellow: fluorine, orange: sulphur, red: oxygen and white: hydrogen.

Figure 6. Calorimetric curve for $[\text{C}_1\text{mim}][\text{NTf}_2]$ obtained using a laboratory-made calorimeter. The scanning rate for cooling and heating was 5 mK/s. The sharp exothermic signal at 283 K during cooling and the endothermic signal at 298 K during heating were assigned to crystallisation and melting, respectively.

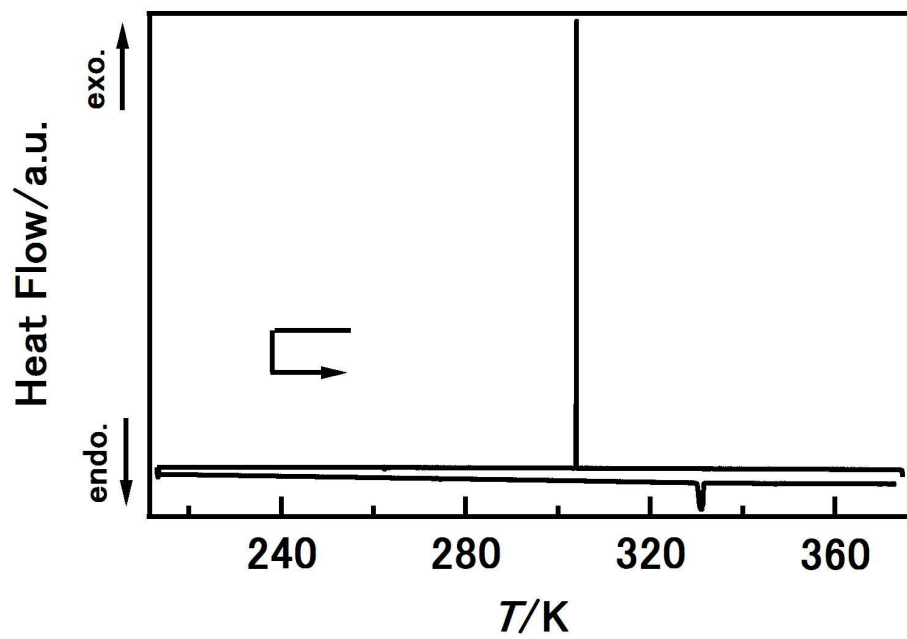
Figure 7. ^{19}F T_1 and T_2 values for $[\text{C}_1\text{mim}][\text{NTf}_2]$ as a function of temperature obtained using a ^{19}F pulse NMR spectrometer. The temperature was varied according to the following cycle: cooling from 393 to 203 K followed by heating to 393 K. Measurements were obtained every 10 K, keeping the temperature constant. The T_1 minimum point could not be clearly recognised after crystallisation.

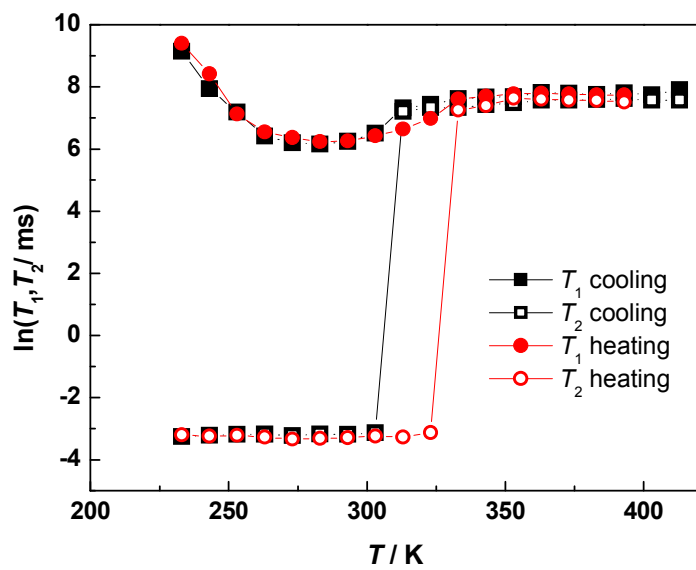
Figure 8. ^1H T_1 and T_2 values for $[\text{C}_1\text{mim}][\text{NTf}_2]$ as a function of temperature obtained using a ^1H pulse NMR spectrometer. The temperature variation was performed in the same manner as described in Figure 7. The minimum point in the T_1 trace for the crystalline state appeared at 213 K.

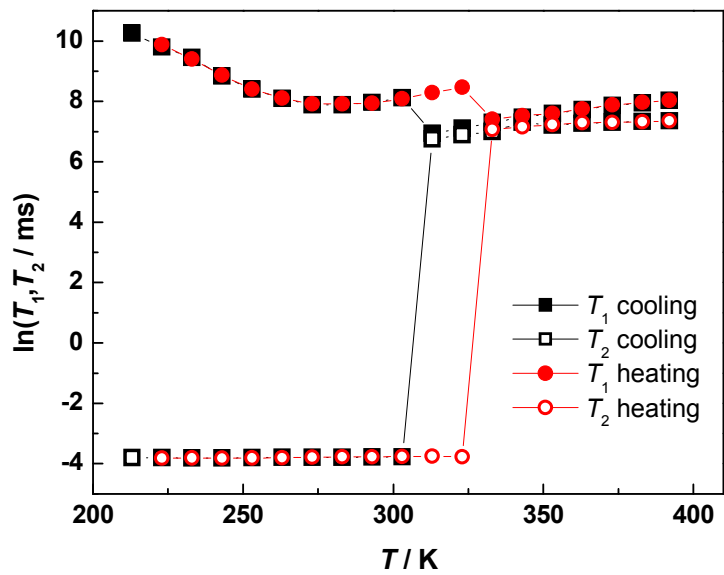
Figure 9. Hydrogen bonding in a $[\text{C}_1\text{mim}][\text{NTf}_2]$ crystal (drawn according to Ref. 66). Grey: carbon, blue: nitrogen, yellow: fluorine, orange: sulphur, red: oxygen and white: hydrogen.

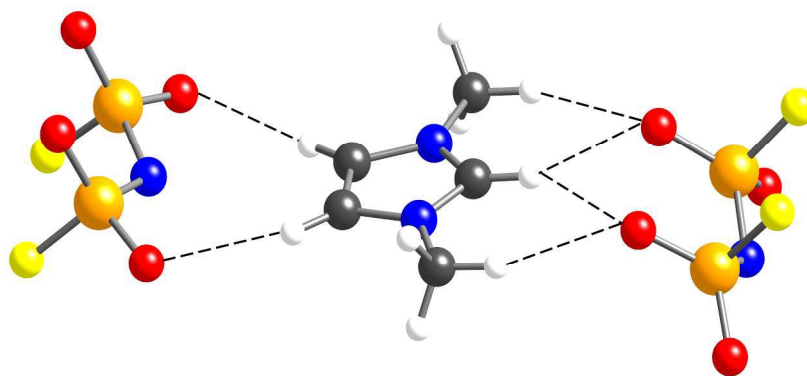


254x190mm (96 x 96 DPI)

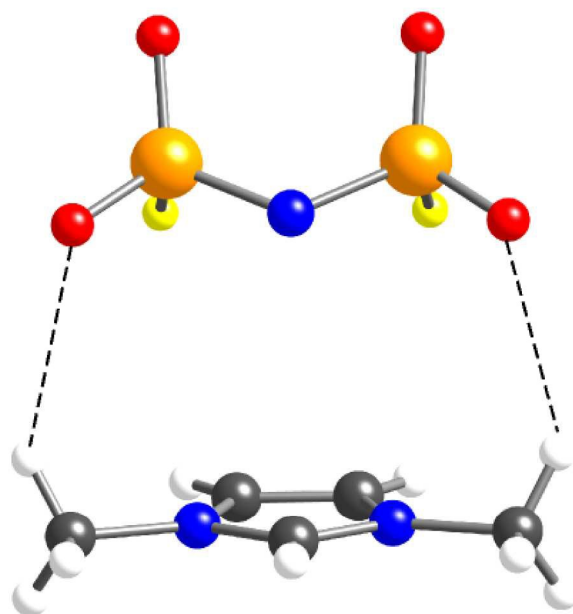








210x297mm (300 x 300 DPI)



210x297mm (300 x 300 DPI)

